Powder Technology 198 (2010) 75–81

Contents lists available at ScienceDirect

Powder Technology

journal homepage: www.elsevier.com/locate/powtec

Numerical study of pleated fabric cartridges during pulse-jet cleaning

Li-Ming Lo [a,*], Shih-Cheng Hu [b], Da-Ren Chen [c], David Y.H. Pui [d]

[a] U.S. Department of Health and Human Services, Public Health Service, Centers for Disease Control and Prevention, National Institute for Occupational Safety and Health, Division of Applied Research and Technology, 4676 Columbia Parkway, MS-R5, Cincinnati, OH 45226, USA
[b] Department of Energy and Refrigerating Air Conditioning, National Taipei University of Technology, Taipei 106, Taiwan
[c] Department of Energy, Environmental & Chemical Engineering, Washington University, St. Louis, MO 63130, USA
[d] Particle Technology Laboratory, Department of Mechanical Engineering, University of Minnesota, Minneapolis, MN 55455, USA

ARTICLE INFO

Article history:
Received 8 January 2009
Received in revised form 8 October 2009
Accepted 16 October 2009
Available online 26 October 2009

Keywords:
Pleated filter cartridge
Pulse-jet cleaning
Computational fluid dynamics analysis
Area-weighted average overpressure

ABSTRACT

We established a numerical model and used computational fluid dynamics (CFD) analysis to observe transient flow behavior across pleated filter cartridges in a dust collector during pulse-jet cleaning. The numerical results were in good agreement with the filter-testing data during important periods including during pressure ramp-up and valve opening. Larger errors for predicting overpressure occurred during the pressure ramp-down period likely due to the uniformity of the filters' permeability. This confirmed that the numerical model demonstrated the cleaning efficiency and the local cleaning quality of three different filter cartridges with different filter dimensions and pleat ratios. Data calculated from the average static pressure on the filters' surfaces were more closely correlated to cleaning efficiency than overpressure. The surface static pressure distribution along all filter cartridges showed that the top area of the filter cartridge is difficult to clean because of the lower surface pressure generated by the pulse jet. Filter cartridges with higher pleat ratios were found to have greater instances of incomplete cleaning due to the large variation of static pressure distribution along the filter cartridges. Our results showed that although information such as average pressure and pressure distribution on the filter surface is difficult to obtain by physical measurement, this data is tractable using CFD analysis and is useful for filter design and system optimization.
Published by Elsevier B.V.

1. Introduction

Two primary filtering and cleaning processes–filtration and back-pulse cleaning–are used in the operation of baghouses or dust collector systems [1–6]. The purpose of this study was to analyze the stable operation of these processes with a focus on pulse-jet-cleaned dust collectors; i.e., we were more concerned about cleaning than filtration.

To design effective pulse-jet pleated filters, understanding the transient flow characteristics–particularly pressure changes across the filter media–of pleated filter cartridges during pulsing is critical. Understanding the pressure distribution on the filter surface during pulse-jet cleaning is also critical to filter design to ensure maximum cleaning efficiency. In both real and in experimental settings, it is difficult to collect this information using physical measurements. Using a numerical analysis simulation model is the only practical way to obtain meaningful measurement data, which will in turn allow one to analyze the transient flow characteristics of a given dust collector system. This measurement data will also allow researchers and designers to conduct a parametric study of various pleated filter designs in order to optimize the operation of a filtration system. In this study, we chose to use computational fluid dynamics (CFD) analysis because we believed it would yield the most accurate and useful data for our study purposes.

Numerical methods have been widely used for understanding the flow behavior of rigid ceramic candle filters and fabric bag filters cleaned by pulse jet. Some studies used simplified one-dimensional models [7,8] to solve the pulse-jet flow in a ceramic filter to optimize filter dimensions and systems design. Other studies used two-dimensional analysis to simulate the transient pulse-jet cleaning process for fabric filter bags [9] and ceramic filters [10,11] to study the design and operating conditions of regenerable filtering systems. A three-dimensional numerical model has also been established to offer more detailed analysis on particle deposition during filtering processes and on pressure distribution on filter media during pulse-jet cleaning [12]. The numerical modeling done by Laux et al. [11] and Ahmadi and Smith [12] using the FLUENT code has demonstrated that the numerical results predicted well the transient pressures exerted on the ceramic filters during backpulse cleaning. Their study also showed that the sharp static pressure gradient across the filter and dust cake appeared to be the main force in removing the dust cake. The static pressure field inside the filter at the initial stage of pulsing, however, had such a nonuniform distribution that it was unable to completely dislodge the cake.

The numerical studies described above provided satisfactory results to analyze, design, and optimize the performance of pulse-jet fabric and ceramic filters, both of which are flat-sheet in shape. In

* Corresponding author. Tel.: +1 513 841 4423; fax: +1 513 841 4506.
E-mail address: LLo@cdc.gov (L.-M. Lo).

0032-5910/$ – see front matter. Published by Elsevier B.V.
doi:10.1016/j.powtec.2009.10.017

contrast, our studies have focused on the use of CFD techniques to analyze the more complicated case of using pleated filter cartridges during backpulse cleaning. In this study, we used numerical analysis to understand the transient variation of surface pressure on pleated filters with different pleat ratios (defined as the ratios of pleat height over pitch), but not using the more costly and time-consuming methods of taking physical experimental measurements.

We know that the accuracy of results from a numerical model can be confirmed by demonstrating the agreement between the model's prediction and experimental observations [13]. Therefore, in the present study we conducted a detailed and fundamental filter test to once again confirm the accuracy of our numerical model. We used the results from our tests using various pressures at the nozzle inlet as inputs for our numerical calculations. The results from the overpressure observed in our experiments using pleated filters during pulsing were used to confirm the numerical model.

2. Methods

2.1. Clean filter testing with pulse jet

Three commercial filter cartridges were used as the test filters for clean filter testing by pulse jet. The filter cartridges are designated as LPR (low pleat ratio at 2.83), MPR (middle pleat ratio at 4.32), and HPR (high pleat ratio at 5.78). The characteristic data of test filters are summarized in Table 1. The test filters were obtained from different manufacturers and vary in filtration area from 3.53 to 5.11 m^2 based on their cartridge dimensions and pleat configurations. The angle of one single pleat from each filter was calculated. This axial symmetry enabled us to create a numerical model for a single pleat which reduced calculation costs.

Fig. 1 shows the experimental setup for conducting the fundamental filter test. The top cover and bottom hopper of the dust collector were removed so that the top and bottom areas were open to the atmosphere. A pressure transducer was installed at the inlet of the nozzle to record gauge pressure variation during pulsing. A differential pressure transducer located at the center location of the filter was used to collect overpressure data across the filter during pulse-jet cleaning. Due to the different dimensions of test filters, the measurement locations of the differential pressure transducer are denoted as (*X1*, *Y*) for the inside of the filter and (*X2*, *Y*) for the outside of the filter. Tank pressure was set at 0.48 MPa to generate a short burst of air to clean the filters. Different pulse durations of 100 ms and 350 ms were used for filter testing.

Table 1
Characteristic data of filters for the numerical study.

Pleated filter cartridge	LPR	MPR	HPR
Pleat height (H, mm)	48	24	35
Pleat pitch (W, mm)	16.96	5.56	6.06
Pleat ratio ($\beta = H/W$)	2.83	4.32	5.78
Inner diameter (D_{in}, mm)	228	159	164
Filter length (L, mm)	629	566	566
Filtration area (A_f, m^2)	3.99	3.53	5.11
Thickness of filter medium (δ_f, mm)	0.8	1	0.35
Angle (θ)	6.00°	3.08°	2.98°

Remarks: Top view of a pleated filter cartridge

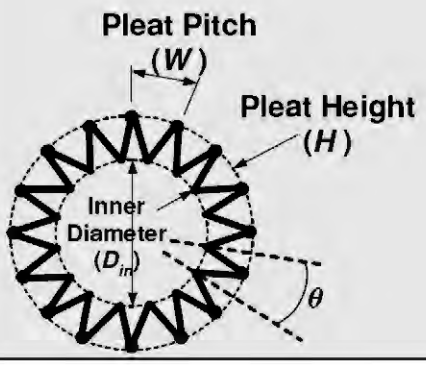

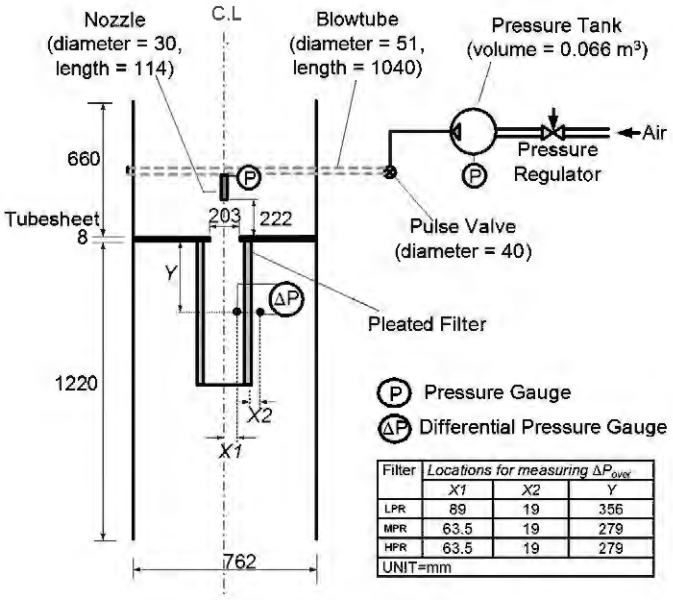

Fig. 1. Schematic diagram of fundamental filter testing.

The filtration process was not active (i.e., 0 cm/s filtration velocity) during the test; this enhanced the precision of the pressure data measurement and simplified the numerical model by excluding the filtering air flow. Our initial test to clean the filters during the normal filtration process showed that obtaining the stable measurement data on transient pressure during pulsing was difficult, particularly at the top opening of the filter cartridges. Similar results have been reported by other studies of ceramic filters [11,14]. The large fluctuation in pressure traces at the filter top is caused by the incomplete mixed nature of the air jet and the strong local velocity and turbulence during the very short time period of the pulse valve open phase. Every testing condition was performed 10 times for each test filter to obtain stable data and reliable results. All the measured data were collected by a digital data acquisition system programmed by LabView software for further analysis. The test data collected were pressure variation over time at the nozzle inlet and transient overpressure (ΔP_{over}) across the filter medium during pulse-jet cleaning under 0.48-MPa tank pressure.

2.2. Computational fluid dynamics (CFD) technique

A commercial code, FLUENT, was employed in this study to develop a numerical model to analyze a pulse-jet-cleaned dust collector. Detailed information about the program is available in the FLUENT User's Guide and in the user-defined function manual. A brief discussion of the FLUENT code, including transportation equations, boundary conditions, and porous media modeling, is provided.

2.2.1. General transport equation

Based on the finite volume method, FLUENT solves the transportation (property conservation) equations enforced in each cell generated in the computational domain. The integral form of the general transportation equation for mass, momentum, energy, etc. is shown as follows:

$$\underbrace{\frac{\partial}{\partial t}\int_V \rho\phi\, dV}_{\text{unsteady}} + \underbrace{\oint_A \rho\phi U\cdot dA}_{\text{convection}} = \underbrace{\oint_A \Gamma\nabla\phi\cdot dA}_{\text{diffusion}} + \underbrace{\int_V S_\phi\, dV}_{\text{generation}} \quad (1)$$

where

V	arbitrary moving volume,
A	surface of the moving volume,
t	time,
U	velocity vector,
Γ	diffusion coefficient,
S_ϕ	source term.

With different inputs for the scalar quantity (ϕ), Eq. (1) can represent specific transportation equations. For example, $\phi = 1$ for the continuity equation; $\phi =$ velocity components (u, v, w) in (x, y, z) coordinates for the momentum equations; $\phi =$ turbulent kinetic energy (κ) or turbulent dissipation rate (e) for the turbulence flow in the κ–e model; $\phi =$ enthalpy for the energy equation; and $\phi =$ mass fraction of species for the species transportation equation. In this numerical work, isothermal flow was assumed so the energy equation was neglected. This is reasonable for analysis of baghouse systems which use fabric filters. No dust was considered in our calculation, i.e., we considered only a single-phase air flow in order to explore the pure effect of pulse-jet cleaning on the filters.

2.2.2. Computation domain and meshing

For our case, we created a numerical model for different filter cartridges installed in a cylindrical dust collector, hence we could use a simple half pleat for numerical calculation because of the pleat's axial symmetry. However, a single pleat model was used in this study to obtain a higher quality mesh on an approximately triangular prism with a sharp angle. As shown in Fig. 2, the angle (θ) was calculated by dividing 360° by the filter pleat number to represent the geometric characteristics of a single pleat. The three-dimensional computation domain included the nozzle, the clean zone (the top portion of the dust collector), the filter cartridge, and the dirty zone (the bottom portion of the dust collector). The schematic diagram of the computation domain is shown in Fig. 3.

The computational domain is an assembly of structured cells. High grid density was placed at the nozzle, at the center location of the filter, and at the upstream and downstream of the pleat to provide greater resolution. The same meshing strategy was used to mesh test filters LPR, MPR, and HPR to generate 83,168; 35,616; and 37,416 cells, respectively. The numerical time step to solve the unsteady backpulse cleaning was about 0.1 to 0.3 ms.

2.2.3. Boundary conditions

Boundary conditions are used in numerical modeling to specify the flow and thermal variables on the boundaries of the physical model. The types of boundary conditions provided by FLUENT can be classified into four categories including (1) faces, (2) double-sided faces, (3) periodic, and (4) cells. The boundary conditions applied in this study (also shown in Fig. 3) are summarized in Table 2 and are briefly described as follows.

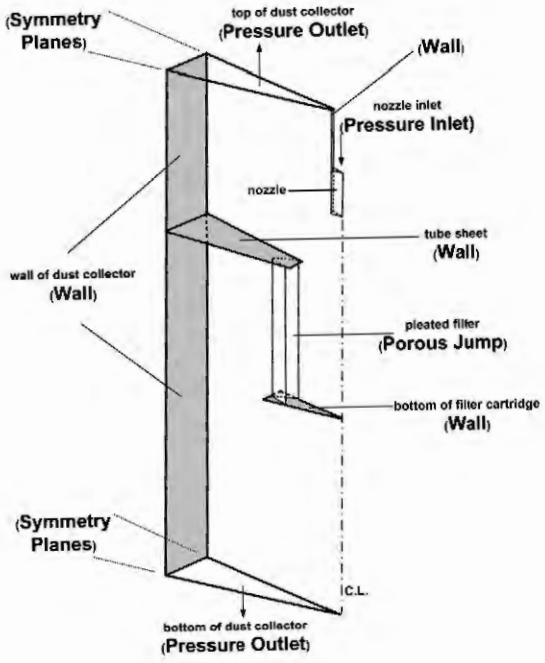

Fig. 3. Schematic diagram of computational domain.

During filter cleaning, the pulse jet enters the dust collector from the nozzle inlet, passes through the pleated filter, and leaves the dust collector from either the top or bottom portions of the dust collector. Pressure inlet conditions were applied at the nozzle inlet, and the value of the transient pressure was specified using a user-defined function based on the filter test data. Pressure outlet conditions at the top and bottom exits of the dust collector were used to specify the atmospheric pressure.

Wall boundary conditions were applied to the solid regions including the wall of the dust collector, at the nozzle, and at the bottom, i.e., the closed end, of the filter cartridge. A no-slip boundary condition is enforced at the walls by default in FLUENT modeling. A single pleat from each filter cartridge was modeled to save computation costs. Zero normal velocity and zero normal gradients of all variables were assumed at the symmetry planes. Air at ambient conditions was used in this study to specify the fluid zone.

In essence, the porous medium is a type of fluid zone. It can be modeled in FLUENT using either porous media conditions or a simplified porous jump model. The porous media model is used to define a "cell" zone so that the pressure loss in the flow can be calculated via the inputs by adding a momentum sink in the governing

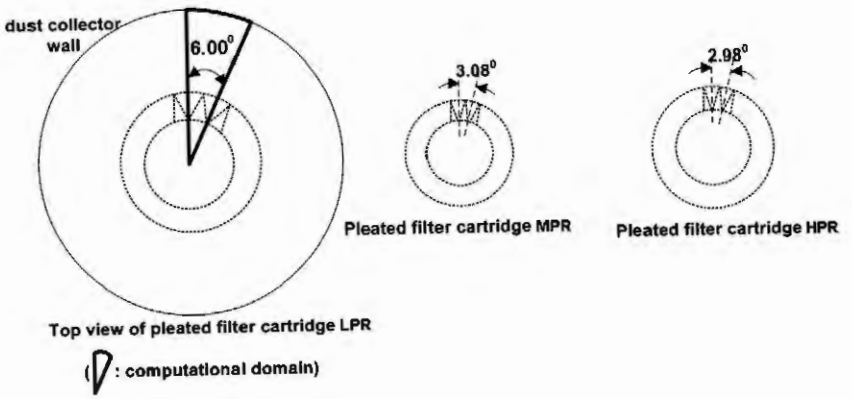

Fig. 2. Schematic diagram of the top view of the LPR, MPR, and HPR filters in the dust collector.

Table 2
Boundary conditions applied in this study.

Category	Zone type
Faces	Pressure inlet, pressure outlet
Double-sided faces	Porous jump, wall
Periodic	Symmetry
Cells	Air

momentum equations. However, the one-dimensional porous jump model applied to a "face" zone provides the advantages of robustness and better convergence, and it was adopted in this work. The details of modeling of porous media are discussed in the next section.

2.2.4. Modeling of porous media

The fluid flow through porous media in FLUENT is modeled by adding a momentum source term (S_i) in the governing equations. The general form of S_i can be expressed as

$$S_i = -\left(\sum_{j=1}^{3} K_{1,ij}\,\mu U_{0,j} + \sum_{j=1}^{3} K_{2,ij}\,\frac{1}{2}\rho|U_{0,j}|U_{0,j}\right) \tag{2}$$

where

S_i source term for the ith (x, y, or z) momentum equation,
K_1 viscous resistance matrix,
K_2 inertial resistance matrix.

Eq. (2) consists of two parts, viscous loss and inertial loss. These losses contribute to the pressure gradient when the fluid flows through the porous media. For simple homogeneous porous media, Eq. (2) can be simplified to give

$$S_i = -\left(k_1\mu U_{0,i} + k_2\frac{1}{2}\rho|U_{0,i}|U_{0,i}\right) = -\left(\frac{\mu}{\alpha}U_{0,i} + k_2\frac{1}{2}\rho|U_{0,i}|U_{0,i}\right) \tag{3}$$

where

k_1 viscous loss coefficient $=\frac{1}{\alpha}$ and
k_2 inertial loss coefficient.

Consider the case of laminar flow through porous media. The effect of inertial resistance is so small that the second term on the right-hand side of Eq. (3) can be neglected. Therefore Eq. (3) can be rewritten in the form of pressure gradient (∇P):

$$-\nabla P = \frac{\mu}{\alpha}U_0 \tag{4}$$

which is known as Darcy's law.

According to Eq. (3), the two resistance factors, k_1 (i.e., α, filter permeability) and k_2, need to be estimated for solving the pressure drop across the pleated filters. Ergun [15] proposed a comprehensive equation to describe the pressure drop (ΔP) due to the flow through beds of granular solids in the following form:

$$\frac{\Delta P}{\delta} = \frac{150(1-\varepsilon)^2}{\varepsilon^3}\frac{\mu}{d_p^2}U_0 + \frac{1.75(1-\varepsilon)}{\varepsilon^3}\frac{\rho}{d_p}U_0^2 \tag{5}$$

where d_p = particle diameter (or fiber diameter when this equation is applied to the porous media), ε = fractional void volume (i.e., porosity) of porous media, and δ = thickness of porous medium.

Eq. (5) is widely applied for modeling different porous media such as fabric filters [16], rigid ceramic filters [17], and dust cakes [18].

Comparing Eq. (5) with Eq. (3), the viscous and inertial loss coefficients become

$$k_1 = \frac{1}{\alpha} = \frac{150(1-\varepsilon)^2}{\varepsilon^3 d_p^2} \tag{6}$$

and

$$k_2 = \frac{3.5(1-\varepsilon)}{\varepsilon^3 d_p}. \tag{7}$$

For most cases, the viscosity resistance (Darcy's Law) is the dominant term in pressure loss across filters or porous media. The inertial resistance term is also considered in the numerical simulation of this study, due to the high-velocity gas flow passing through the filter during backpulsing.

Referring to ASTM Standard D737-04 [19], the estimated permeability of our test filters while introducing clean air into the dust collector to measure the pressure drops could be determined by Darcy's Law. In this study, constants α and k_2 were required as inputs for calculating the flow through pleated filter cartridges because of the limitation of FLUENT. The calculation error could be generated from constant settings of α and k_2 since both coefficients are a function of the filter medium structure (ε), which might be influenced by a high-speed pulse jet. Therefore, our strategy for model confirmation was to first use a smaller k_2 in order to make α the main contributor to the pressure drop and then adjusting α only enough to obtain numerical results that matched the filter-testing data. A constant k_2 of 1000 was used for all calculation cases. In this work, we also assumed that there was no interaction between the fluid and the porous media, and any deformation of the filter media during pulsing was neglected.

3. Results and discussion

The most important step after the establishment of a model is to demonstrate its effectiveness and reliability. The model can be confirmed by checking the deviation between observation (filter-testing data) and predication (numerical output) [13]. The purpose of this study was to use our confirmed model to obtain numerical values for the static pressure on a filter's surface. By using this data to demonstrate the relationship between cleaning efficiency and filter geometry, we hope that our work might provide useful information for the air filtration industry and help designers and engineers improve pleated filter design and optimize pulse-jet systems.

3.1. Filter test results

Compressed air was delivered through a blowtube to the nozzle for filter cleaning. The pressure variation at the nozzle inlet was recorded by a pressure transducer as depicted in Fig. 4. The pressure at the nozzle inlet reached the maximum value (45,000 Pa in our case when tank pressure at 0.48 MPa was used) in 150 ms, then continuously decreased. The total time to complete a pulse cleaning was 520 ms for the short pulse duration (t_p = 100 ms), and 760 ms for the long pulse duration (t_p = 350 ms). The time characteristics shown in Fig. 4 are summarized in Table 3. Due to the similar behavior of short and long pulse durations, only the case of the 100-ms pulse duration was simulated in this study, and pressure variation at this pulse duration was used as an input condition for numerical calculations.

We expected that the pressure response across the test filters (i.e., overpressure variation) would be similar to the pressure at the nozzle inlet during pulse-jet cleaning. The test results of overpressure variations across all test filters are depicted in Fig. 5. The magnitude of overpressure shown for different test filters mainly depended on the filter's characteristics such as dimensions, pleat ratio, and material. Given the same cleaning conditions, the MPR filter generated higher overpressure (1100 Pa) than the LPR (700 Pa) and HPR filters (200 Pa).

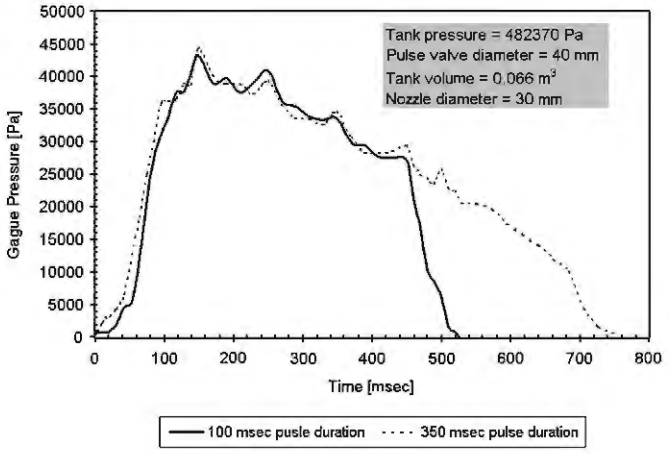

Fig. 4. Transient gauge pressure at the nozzle inlet during pulsing.

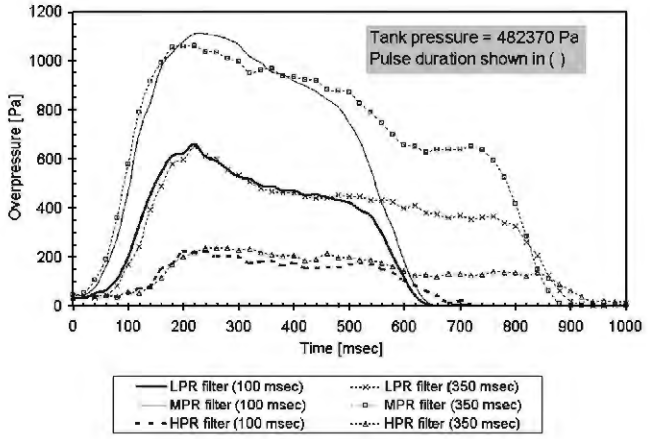

Fig. 5. Transient overpressure (ΔP_{over}) across the center locations along test filters during pulsing.

The experimental data shown in Fig. 5 were used to compare with the numerical data to confirm the numerical model.

As shown in Fig. 4, the peak pressure of the air jet at the nozzle inlet was about 45,000 Pa. This demonstrates that the Mach number in the clean zone was less than 1, which justifies the assumption of incompressible flow in this study.

3.2. Confirmation of our numerical model

Fig. 6 summarizes the transient overpressure data across test filters from experimental measurements and from numerical simulations under pulsing with 0.48-MPa tank pressure and a 100-ms pulse duration. (Refer to Fig. 1 for the measurement locations across the filters.) The values of the best-fit permeability of the LPR, MPR, and HPR filters for numerical calculation were 1.95×10^{-12}, 3.5×10^{-12}, and 1.0×10^{-12}, respectively. The calculated and experimental results showed good agreement, but a larger deviation was found after 500 ms (i.e., the pressure ramp-down period), demonstrating that the assumption of constant filter permeability is not appropriate for the entire duration of pulsing. A similar study showed that filter permeability could be increased by the entrained secondary air flow where primary air is constant [20]. A similar conclusion was found from a numerical study of ceramic candle filters which showed that a candle filter could have variable permeability during pulsing depending on its location [3]. Overall, our numerical model still captured the most important behaviors of overpressure changes during pressure ramp-up and during open-valve periods when pulse-jet cleaning.

3.3. Average static pressure on filter surface ($\overline{P_s}$) during pulsing

We were able to calculate very detailed data regarding transient flow behavior across the filters from our confirmed numerical model. Let $\overline{P}_s(x, y, z)$ denote the static pressure distribution on the filter surface. Here the x direction refers to the position along the filter height and y and z represent the locations on the filter pleat. The overall average static pressure on the filter surface at time t, $\overline{P}_s|_t$ can be computed as follows:

$$\overline{P_s}|_t = \frac{\sum P_s(x,y,z)|_t}{m} \tag{8}$$

where

$P_s(x, y, z)|_t$ static pressure at the node (x, y, z) at time t,
m total number of nodes.

According to our simulation results, the pressure variation during pulsejet cleaning was only found to be significant along the x-coordinate (i.e., along the traveling direction of the pulse jet).

When measuring the cleaning efficiency of pulse-jet-cleaned filters, the static pressure on the filter surface is more meaningful than overpressure data [21], particularly for the case of pleated filters. The variation in the cleaning effectiveness of our test filter cartridges according to the average static pressure on the individual surfaces ($\overline{P}_s$) of the filters is shown in Fig. 7. A filter's ability to dislodge a surface dust cake depends on its peak static pressure ($\overline{P_{s,max}}$), hence we used it as an indication of a filter's cleaning ability. At a cleaning intensity of 0.48-MPa tank pressure and a 100-ms pulse duration, the MPR filter reached a peak static pressure of near 400 Pa on its surface. At the same cleaning intensity, the HPR filter generated only about 50 Pa. These findings suggest that unless an alternative process (e.g., changing the flexibility

Table 3
Summary of time characteristics of short and long pulse durations.

Pulse duration (t_p)	100 ms	350 ms
Pressure ramp-up time (τ_{up})	150 ms	150 ms
Time interval of valve open (τ_{open})	300 ms	550 ms
Pressure ramp-down time (τ_{down})	70 ms	60 ms
Total time	520 ms	760 ms

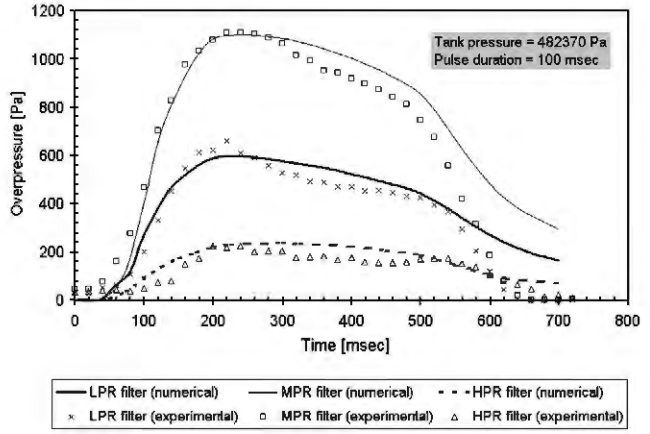

Fig. 6. Calculated and measured transient overpressure (ΔP_{over}) across the center locations along test filters during pulsing.

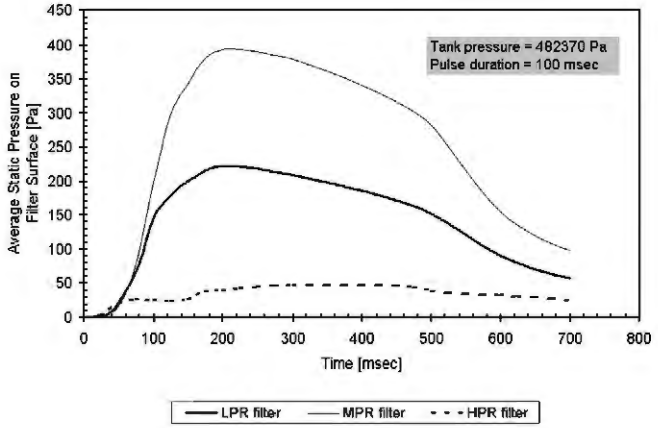

Fig. 7. Calculated transient pressures on the surface of test filters ($\overline{P}_s$) during pulsing.

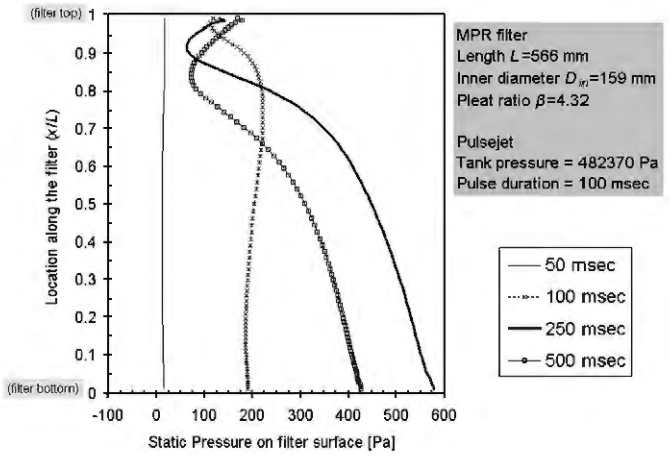

Fig. 9. Calculated transient pressures during pulsing at various locations ($\overline{P}_s(x, y, z)$) along the MPR filter.

of filter material to enhance the acceleration during backpulse cleaning) is used to increase cleaning intensity, an increase in cleaning frequency is required to maintain comparative cleaning levels in filters with relatively high pleat ratios [22]. The peak static pressure on the surface of the LPR filter, which had a much larger inner diameter, reached near 225 Pa. This pressure was lower than that generated by the MPR filter but higher than that generated by the HPR filter, both of which had a higher pleat ratio and a similar or larger filtration area than the LPR filter. Based upon our $\overline{P}_s$, we concluded that $\overline{P_{s,max}}$ depends on both the number of pleats and the dimensions of the filter cartridge. These findings have led us to a new numerical study to explore how the structure of filter pleats influences a filter cartridge's cleaning efficiency. This work will be discussed in our next paper.

3.4. Static pressure distribution on filter surfaces ($P_s(x,y,z)$) during pulsing

The pressure distribution along a filter's surface during pulsing is useful information when evaluating a filter's cleaning quality along and across all areas of the filter's surface. Humphries and Madden [2] measured the pulse pressure inside the filter bag to establish the relationship between average pulse pressure and the fraction of dust dislodged. They found that a nonuniform peak pressure along the length of the filter bag caused only partial dislodgement of the dust cake. The filter could not be cleaned completely until a critical tank pressure was used. Similar results were found by Sievert and Loffler [21]. Both studies showed similar characteristics of the effect of peak static pressure on the various locations in the filter bag. The lowest static pressure was found along the top portion of the filter after the pulse jet struck the filter bag, while the pressure tended to increase near the bottom portion of the filter due to the reflection of the pulse. Our confirmed numerical model allows us to determine the pressure distribution along a filter's surface to demonstrate how surface pressure varies according to location in pleated filter cartridges. (See Figs. 8–10 for LPR, MPR, and HPR filters, respectively.) In our model, we used the dimensionless parameter x/L to characterize the location of the filter cartridge. $x/L=1$ represents the top location of filters, and $x/L=0$ the bottom location.

Our finding that pressure tends to vary among the different locations of a pleated filter cartridge during pulsing is similar to findings from previous studies of filter bags [2,21]. In general, the lowest static pressure on the pleated filter cartridges was found at $x/L=0.8$, and the highest static pressure was found at the bottom. This indicates that $x/L = 0.8$ is a vulnerable spot with a high potential for incomplete cleaning. The slopes of the pressure distribution are shown in Figs. 8–10. Higher pleat ratios produce steeper pressure distributions during pulsing, suggesting that incomplete cleaning is more likely in filter cartridges with high pleat ratios because of the high variation in the static pressure distribution along the filter cartridge. Given the same cleaning intensity, filter cartridges with high pleat ratios should be cleaned by the clean-on-time mode, which uses a shorter and fixed-time cleaning interval. As demonstrated in our experimental study [22], the use of the clean-on-time mode would likely remedy the problem of incomplete cleaning associated with high pleat ratio filters during long-term operation of a dust collector.

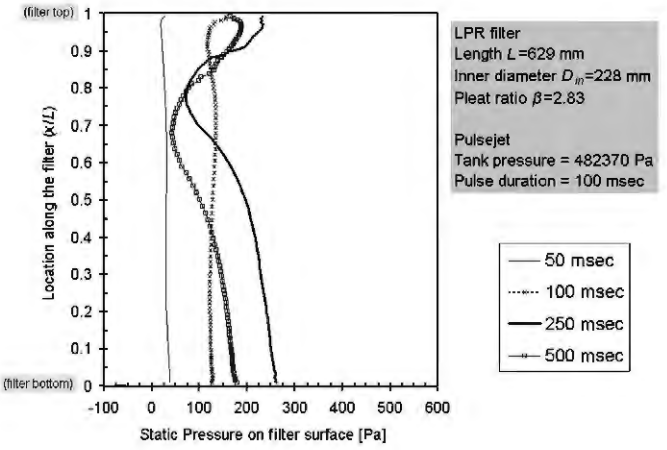

Fig. 8. Calculated transient pressures during pulsing at various locations ($\overline{P}_s(x, y, z)$) along the LPR filter.

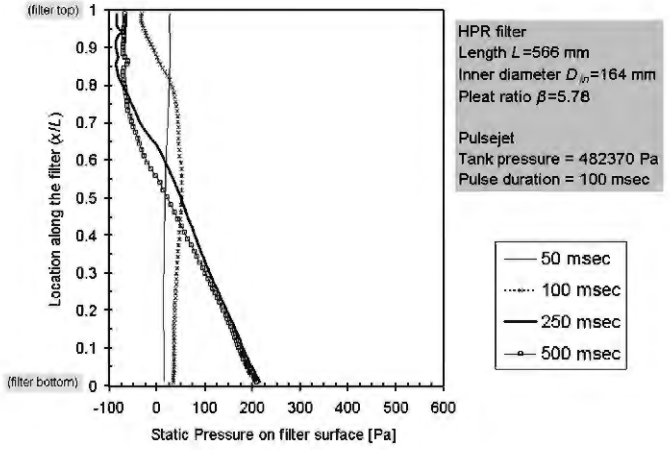

Fig. 10. Calculated transient pressures during pulsing at various locations ($\overline{P}_s(x, y, z)$) along the HPR filter.

4. Conclusions

In this study, we developed a numerical model to analyze pleated filter cartridges during pulse-jet cleaning and confirmed our model by comparing experimental data gathered from fundamental filter testing. With the model, we were able to obtain information not obtainable using experimental measurements.

Any errors in our numerical model in predicting the comprehensive data of overpressure during pulsing were caused by the limiting assumption of uniform filter permeability. Still, our results showed that the model could predict overpressure variation during important periods, such as during pressure ramp-up and at valve opening, with acceptable accuracy. Our numerical results show that filter permeability varies during pulsing and increases during pulse-jet cleaning. Since there is such a strong dependence of filter permeability upon cleaning efficiency, our results demonstrate that numerical simulation may be useful for designers when considering the effect of filter permeability on cleaning efficiency.

To analyze pleated filter cartridges, the average static pressure on the filter surface ($\overline{P}_s$) is a better indication of cleaning efficiency than overpressure, hence the information predicted by our numerical model provided an important design rule for pulse-jet-cleaned filter cartridges. Information from our model regarding static pressure distribution along a clean filter cartridge ($\overline{P}_s(x, y, z)$) can explain the test results of pleated filters challenged by hydrated alumina dust [22]. Also it should help filter designers inspect the cleaning quality along and across the filter's surface. As demonstrated in several of the previous studies cited, we found that the surface pressure along a filter cartridge decreases toward the top of the cartridge and increases gradually near the bottom. Consequently, determination of the slope of the surface pressure distribution is important when choosing the appropriate cleaning mode for pleated filter cartridges. These findings, together with the remaining question of how the structure of filter pleats influences a filter cartridge's cleaning efficiency, will be explored in our future paper.

Disclaimer

Mention of company names and/or products does not constitute endorsement by the Centers for Disease Control and Prevention (CDC). The findings and conclusions in this report are those of the authors and do not necessarily represent the views of the National Institute for Occupational Safety and Health (NIOSH).

Acknowledgements

The authors thank the support of members of the Center for Filtration Research: 3 M Corporation, Cummins Filtration Inc., Donaldson Company, Inc., E. I. du Pont de Nemours and Company, Entegris Inc., Samsung Semiconductor Inc., Shigematsu Works CO., LTD, TSI Inc., and W. L. Gore & Associates and the affiliate member National Institute for Occupational Safety and Health (NIOSH). Special appreciation is given to W. L. Gore & Associates, Inc. and Donaldson Company, Inc. for their help in filter testing.

We also acknowledge NIOSH colleagues including Jennifer Topmiller, Scott Earnest, James Bennett, Benjamin Eimer, and Chaolong Qi for their critical review of the manuscript, and thank Douglas Platt for his useful editing.

References

[1] D. Leith, M.J. Ellenbecker, Theory for pressure drop in a pulse-jet cleaned fabric filter, Atmos. Environ. 14 (1980) 845–852.
[2] W. Humphries, J.J. Madden, Fabric filtration for coal-fired boilers: dust dislodgement in pulse jet filters, Filtr. Sep. (January/February 1983) 40–44.
[3] K.T. Hindy, Influence of selected fixed parameters on pulse-jet fabric filter operation, Atmos. Environ. 20 (1986) 1517–1521.
[4] H.C. Lu, C.J. Tsai, A pilot-scale study of the design and operation parameters of a pulse-jet baghouse, Aerosol. Sci. Tech. 29 (1988) 510–524.
[5] C. Kanaoka, T. Kishima, Observation of the process of dust accumulation on a ridge ceramic filter surface and the mechanism of cleaning dust from the filter surface, Adv. Powder Technol. 10 (1999) 417–426.
[6] H. Leubner, U. Riebel, Pulse jet cleaning of textile and rigid filter media-characteristic parameters, Chem. Eng. Technol. 27 (2004) 652–661.
[7] S. Ito, Pulse jet cleaning and internal flow in a large ceramic tube filter, in: R. Clift, J.P.K. Seville (Eds.), Gas Cleaning at High Temperatures, Blackie Academic and Professional Publishers, New York, 1993, pp. 266–279.
[8] Z. Ji, M. Shi, F. Ding, Transient flow analysis of pulse-jet generation system in ceramic filter, Powder Technol. 139 (2004) 200–207.
[9] H.C. Lu, C.J. Tsai, Numerical and experimental study of cleaning process of a pulse-jet fabric filtration system, Environ. Sci. Technol. 30 (1996) 3243–3249.
[10] Z. Ji, S. Peng, L. Tan, Numerical analysis of flow field in ceramic filter during pulse cleaning, Chin. J. Chem. Eng. 11 (2003) 626–632.
[11] S. Laux, B. Giernoth, H. Bulak, U. Renz, Aspects of pulse-jet cleaning of ceramic filter elements, in: R. Clift, J.P.K. Seville (Eds.), Gas Cleaning at High Temperatures, Blackie Academic and Professional Publishers, New York, 1993, pp. 203–224.
[12] G. Ahmadi, D.H. Smith, Analysis of steady-state filtration and backpulse process in a hot-gas filter vessel, Aerosol Sci. Tech. 36 (2002) 665–677.
[13] N. Oreskes, K. Shrader-Frechette, K. Belitz, Verification, validation, and confirmation of numerical models in the earth sciences, Science 263 (1994) 641–646.
[14] S. Berbner, F. Loffler, Pulse jet cleaning of rigid filter elements at high temperature, in: R. Clift, J.P.K. Seville (Eds.), Gas Cleaning at High Temperatures, Blackie Academic and Professional Publishers, New York, 1993, pp. 225–243.
[15] S. Ergun, Fluid flow through packed columns, Chem. Eng. Prog. 48 (1952) 89–94.
[16] I.F. Macdonald, M.S. El-Sayed, K. Mow, F.A.L. Dullien, Flow through porous media—the Ergun equation revisited, Ind. Eng. Chem. Fund. 18 (1973) 199–208.
[17] J.P.K. Seville, R. Clift, C.J. Withers, W. Keidel, Rigid ceramic media for filtering hot gases, Filtr. Sep. (July/August 1983) 265–271.
[18] M.L. Aguiar, J.R. Coury, Cake formation in fabric filtration of gases, Ind. Eng. Chem. Res. 35 (1996) 3637–3679.
[19] ASTM D737-04, Standard Test Method for Air Permeability of Textile Fabrics, ASTM International, 2008, doi:10.1520/D0737-04R08E01, 5 pps.
[20] E. Bakke, Optimizing filtration parameters, JAPCA J. Air Waste Manage. 24 (1974) 1150–1154.
[21] J. Sievert, F. Loffler, Fabric cleaning in pulse-jet filters, Chem. Eng. Proc. 262 (1989) 179–183.
[22] L.M. Lo, D.R. Chen, D.Y.H. Pui, Experimental study of pleated fabric cartridges in a pulse-jet cleaned dust collector, Powder Technol. (2010) 141–149.